

# Thermal Starless Ammonia Core Surrounded by CCS in the Orion A Cloud

Ken'ichi Tatematsu,<sup>1,2</sup> Tomoya Hirota,<sup>1,2</sup> Satoshi Ohashi,<sup>3</sup> Minhoo Choi,<sup>4</sup> Jeong-Eun Lee,<sup>5</sup>  
Satoshi Yamamoto,<sup>6</sup> Tomofumi Umemoto,<sup>1,2</sup> Ryo Kandori,<sup>1</sup> Miju Kang,<sup>4</sup>

and

Norikazu Mizuno<sup>1,3</sup>

Received \_\_\_\_\_; accepted \_\_\_\_\_

---

<sup>1</sup>National Astronomical Observatory of Japan, 2-21-1 Osawa, Mitaka, Tokyo 181-8588, Japan; k.tatematsu@nao.ac.jp, tomoya.hirota@nao.ac.jp, umemoto.tomofumi@nao.ac.jp, r.kandori@nao.ac.jp, norikazu.mizuno@nao.ac.jp

<sup>2</sup>Department of Astronomical Science, The Graduate University for Advanced Studies (SOKENDAI), 2-21-1 Osawa, Mitaka, Tokyo 181-8588, Japan

<sup>3</sup>Department of Astronomy, The University of Tokyo, Bunkyo-ku, Tokyo 113-0033, Japan; satoshi.ohashi@nao.ac.jp

<sup>4</sup>Korea Astronomy and Space Science Institute, Daedeokdaero 776, Yuseong, Daejeon 305-348, South Korea; minho@kasi.re.kr, mj Kang@kasi.re.kr

<sup>5</sup>School of Space Research, Kyung Hee University, Seocheon-Dong, Giheung-Gu, Yongin-Si, Gyeonggi-Do, 446-701, South Korea; jeongeun.lee@khu.ac.kr

<sup>6</sup>Department of Physics, The University of Tokyo, Bunkyo-ku, Tokyo 113-0033, Japan; yamamoto@taurus.phys.s.u-tokyo.ac.jp

## ABSTRACT

We imaged two starless molecular cloud cores, TUKH083 and TUKH122, in the Orion A giant molecular cloud in the CCS and ammonia ( $\text{NH}_3$ ) emission with the Very Large Array. TUKH122 contains one  $\text{NH}_3$  core “TUKH122-n,” which is elongated and has a smooth oval boundary. Where observed, the CCS emission surrounds the  $\text{NH}_3$  core. This configuration resembles that of the  $\text{N}_2\text{H}^+$  and CCS distribution in the Taurus starless core L1544, a well-studied example of a dense prestellar core exhibiting infall motions. The linewidth of TUKH122-n is narrow ( $0.20 \text{ km s}^{-1}$ ) in the  $\text{NH}_3$  emission line and therefore dominated by thermal motions. The smooth oval shape of the core boundary and narrow linewidth in  $\text{NH}_3$  seem to imply that TUKH122-n is dynamically relaxed and quiescent. TUKH122-n is similar to L1544 in the kinetic temperature (10 K), linear size (0.03 pc), and virial mass ( $\sim 2 M_\odot$ ). Our results strongly suggest that TUKH122-n is on the verge of star formation. TUKH122-n is embedded in the 0.2 pc massive (virial mass  $\sim 30 M_\odot$ ) turbulent parent core, while the L1544  $\text{NH}_3$  core is embedded in the 0.2 pc less-massive (virial mass  $\sim 10 M_\odot$ ) thermal parent core. TUKH083 shows complicated distribution in  $\text{NH}_3$ , but was not detected in CCS. The CCS emission toward TUKH083 appears to be extended, and is resolved out in our interferometric observations.

*Subject headings:* ISM: clouds —ISM: individual (Orion Nebula, Orion Molecular Cloud) —ISM: molecules —ISM: structure—stars: formation

## 1. Introduction

“Giant molecular clouds (GMCs)” are known to form star clusters with both massive and low-mass stars while “cold dark clouds” (also called “nearby dark clouds”, “small molecular clouds”, or “SMCs”; excluding “infrared dark clouds” here) can form only low-mass stars in isolation (e.g. Shu et al. 1987; Turner 1988; Bergin & Tafalla 2007). These two categories of molecular clouds have different physical properties. Molecular clouds have hierarchical structure, and structures having sizes of the order 0.1 pc are often called “molecular cloud cores” or simply “cores.” The nonthermal motion or turbulence is dominant in cores in GMCs, while the thermal motion is more dominant in cores in cold dark clouds (e.g. Turner 1988; Tatematsu et al. 1993; Caselli & Myers 1995). Because most stars in the Galaxy form in GMCs, star formation from their cores is of great interest. How do stars form from turbulent cores in GMCs? Do turbulent cores dissipate turbulence partially or completely before star formation? Therefore, it is essential to observationally characterize cores in GMCs in the turbulent environments where most stars are born. It was theoretically suggested that cores are dynamical rather than quasistatic objects with relatively short lifetimes (e.g. Ballesteros-Paredes et al. 2003, 2007). If this is true, cores in GMCs cannot be quasistatic, and will be far different from quiescent cores in cold dark clouds (e.g. Myers 1983; Pineda et al. 2011). Some researchers have pointed out that the dissipation of turbulence can initiate the star formation process (Myers 1983; Nakano 1998; Aso et al. 2000). However, it is not well established observationally how turbulent molecular clouds form stars. We wonder whether stars form in dynamical cores or quiescent cores, whether turbulence dissipates before star formation, and how it does. To know how star formation occurs in GMCs, it is essential to investigate starless molecular cloud cores that might lead to star formation in near future in detail.

We take the Orion A cloud, which is the nearest and best studied GMC (e.g.

Genzel & Stutzki 1989). The overall structure is filamentary, and contains the “f-shaped filament” (0.5 pc wide, 13 pc long) in the northern region (Bally et al. 1987). Johnstone & Bally (1999) mapped the f-shaped filament at 450 and 850  $\mu\text{m}$ , and found a chain of compact sources along a narrow ( $< 0.14$  pc) high-density filament. The Orion A GMC has a hierarchical structure consisting of 1.4 pc-width filaments (Nagahama et al. 1998) as well as 1 pc-sized clumps and 0.1 pc-sized cores (Batra et al. 1983; Bally et al. 1987; Castets et al. 1990; Tatematsu et al. 1993; Cesaroni & Wilson 1994; Chini et al. 1997; Tatematsu et al. 1998; Lis et al. 1998; Aso et al. 2000; Johnstone & Bally 2006; Ikeda et al. 2007; Tatematsu et al. 2008; Takahashi et al. 2013).

To identify candidate starless cores close to star formation, we use chemical evolution tracers. Tatematsu et al. (1993) mapped the Orion A GMC in CS  $J = 1-0$  with the Nobeyama 45 m radio telescope, and cataloged 125 cores (we use the prefix of TUKH). Tatematsu et al. (2010) made single-pointing observations toward more than 60 TUKH cores in CCS and other molecules with the Nobeyama 45 m radio telescope. They detected CCS in molecular cloud cores in the Orion A GMC for the first time; this molecule is known as a tracer of young molecular gas in cold dark clouds through observations and chemical model calculations (Suzuki et al. 1992). TUKH122 and TUKH083 are the most and second-most intense cores in CCS  $J_N = 4_3 - 3_2$ , respectively, in their observations. From their data, TUKH083 is thought to be a young starless core, because it meets the category of the Carbon-Chain-Producing Regions (CCPRs) on the  $N(\text{CCS})$ - $N(\text{NH}_3)$ / $N(\text{CCS})$  diagram defined by Hirota, Ohishi, & Yamamoto (2009). On the other hand, TUKH122 is thought to be an older starless core, because it is not categorized in the CCPRs category. Tatematsu et al. (2014) mapped six TUKH cores in the Orion A GMC in  $\text{N}_2\text{H}^+$   $J = 1-0$  and CCS  $J_N = 7_6 - 6_5$  also with the Nobeyama 45 m telescope, and identified sub-peaks in these lines. They confirmed that the column density ratio of  $\text{N}_2\text{H}^+$  to CCS can be used as a chemical evolution tracer even in the GMCs if the gas temperature in the core

does not exceed  $\sim 25$  K. The  $\text{N}_2\text{H}^+$  sub-peaks (TUKH122C and TUKH122D) inside the TUKH122 region have the largest  $N(\text{N}_2\text{H}^+)/N(\text{CCS})$  column density ratios (2–3) among the starless sub-peaks observed by Tatematsu et al. (2014). The ratios are close to the criterion between starless and star-forming core peaks, which means these sub-peaks are close to star formation. TUKH122 has the narrowest  $\text{N}_2\text{H}^+$  line profiles in their  $\text{N}_2\text{H}^+$  core samples. In this study, we mapped two starless cores TUKH083 and TUKH122 in the Orion A GMC, by observing the ammonia ( $\text{NH}_3$ ) and CCS emission to investigate the physical and chemical properties. According to Wilson et al. (1999), TUKH083 and TUKH122 have  $\text{NH}_3$  rotational temperatures of 35 and  $< 15$  K, respectively. These correspond to the kinetic temperature  $T_K = 60$  K and  $< 15$  K, respectively by using the conversion given by Danby et al. (1988). Wilson et al. (1999) obtained  $T_K$  also from CO  $J = 3-2$  peak intensities to be 15 and 12 K for TUKH083 and TUKH122, respectively. When we investigate the Herschel Observatory images, the dust continuum emission corresponding to TUKH122 is seen in Figure 2 of Roy et al. (2013), but that corresponding to TUKH083 is not clear in Figure 10 of Lombardi et al. (2014) probably due to confusion in a crowded region. According to Figure 2 of Roy et al. (2013), the dust temperature toward TUKH122 is approximately 12–13 K.

In this work we adopt a distance of  $418 \pm 6$  pc based on the work of Kim et al. (2008) as the best estimate; at this distance 1' corresponds to 0.12 pc

## 2. Observations

Observations were carried out by using the Karl G. Jansky Very Large Array (hereafter VLA) of the National Radio Astronomy Observatory<sup>1</sup> of the United States of America in the D configuration. The observation dates are five days between 2010 August 29 and 2010 September 9. We observed  $\text{NH}_3$  ( $J, K$ ) = (1, 1) at 23.694495 GHz (Ho & Townes 1983) and CCS  $J_N = 4_3 - 3_2$  at 45.379033 GHz (Yamamoto et al. 1990) in both of the right-hand and left-hand circular polarizations, simultaneously. We employed the receiver front-ends for 1.3 cm K band and 0.7 cm Q band. The tracking velocity was  $v_{LSR-K} = 4.0 \text{ km s}^{-1}$ . The receiver back-end was the WIDAR correlator in the OSRO2 mode. The channel width was 15.625 kHz (corresponding to  $0.197 \text{ km s}^{-1}$ ) for  $\text{NH}_3$  and 31.25 kHz (corresponding to  $0.207 \text{ km s}^{-1}$ ) for CCS. The number of the frequency channels was 256. We observed 3C147 as the flux and bandpass calibrator. The observed intensity is reported in terms of  $\text{Jy beam}^{-1}$ . We used J0541-0541 as the phase calibrator. Immediately before the flux, bandpass, and phase calibration, we made pointing observations in X band toward the same calibrators. Tables 1 and 2 list observation sessions and observational parameters. The observed data were flagged, calibrated, and imaged (CLEANed) using the CASA 4.1 software package. The flux of the flux calibrator 3C147 is assumed to be 1.783 Jy at K band and 1.0136 Jy at Q band, from the model of “Perley-Butler 2010” in CASA. The CLEAN deconvolution was made using the simple Clark Algorithm with the natural weighting and with UV taper. For Q-band observations, we applied the Gaussian filter of “outertaper” =  $3''.0$  in addition in the CLEAN deconvolution. The primary beam size was about  $2'$  for K band and  $1'$  for Q band. We used the software package AIPS to plot images and spectra to be presented in this paper. Figures 1 and 2 show the primary beams of our interferometric observations

---

<sup>1</sup>The National Radio Astronomy Observatory is a facility of the National Science Foundation operated under cooperative agreement by Associated Universities, Inc.

at K band toward TUKH083 and TUKH122 superimposed on the CS  $J = 1-0$  maps of Tatematsu et al. (1993). All the interferometric maps are corrected for the primary beam response.

### 3. Results

Core TUKH122 was clearly detected in both the  $\text{NH}_3$  and CCS emission. Core TUKH083 was detected only in the  $\text{NH}_3$  emission. We have not detected the continuum emission either in K or Q bands. The  $3\sigma$  upper limit to the continuum emission is 1.56 mJy beam $^{-1}$  or 0.276 K for K band and 5.4 mJy beam $^{-1}$  or 0.189 K for Q band.

#### 3.1. TUKH122 map

Figures 3 to 5 show  $\text{NH}_3$  and CCS velocity-integrated intensity maps toward TUKH122. Figure 4 shows the  $\text{NH}_3$  map. The  $\text{NH}_3$  map shows the emission distribution elongated in the northwest-southeast direction. The boundary shape is very smooth and oval. The  $\text{NH}_3$  emission roughly corresponds to the  $\text{N}_2\text{H}^+$  emission observed by Tatematsu et al. (2014) as TUKH122C and D. The noise level increases outward, because the primary beam response is corrected. All the features outside the primary beam size are noise rather than the emission. The  $\text{NH}_3$  core has some internal structure, and the southeastern side of the  $\text{NH}_3$  core looks clumpy. It might be affected by higher noise level near the edge of the primary beam to some extent, but it is likely that some internal structures are real. We call the overall core TUKH122-n, and internal sub-cores TUKH122-n1 and n2. The direction of the elongation of TUKH122-n is more or less in parallel with the CS filament (P.A.  $\sim 135^\circ$ ) having a width of  $\sim 0.1$  pc in Figure 2. Table 3 lists the physical parameters of TUKH122-n, n1, and n2. We fit two-dimensional Gaussians to the emission distribution,

and derive the beam-deconvolved parameters.  $a$ ,  $b$ , and PA are the major and minor diameters, and the position angle, respectively. The axial ratio (minor diameter/major diameter) is 0.26, which is smaller than the typical value in cores in cold dark clouds, on the order 0.5 (Myers et al. 1991). This core elongation is also in parallel with the global filamentary shape (e.g. Bally et al. 1987; Tatematsu et al. 1993) of the Orion A GMC. The flux of the core TUKH122-n obtained through the spatial two-dimensional Gaussian fitting is  $392 \text{ mJy km s}^{-1}$ . Using the MPIfR 100m radio telescope, Wilson et al. (1999) observed TUKH122 in  $\text{NH}_3$ , and obtained a main-beam radiation temperature of  $T_R = 2.28 \text{ K}$  and an FWHM linewidth of  $0.8 \text{ km s}^{-1}$ , resulting in an integrated intensity of  $1.94 \text{ K km s}^{-1}$ . This corresponds to  $1.64 \text{ Jy km s}^{-1}$  in their  $43''$  beam. Then, 24% of the single dish flux was resolved with the VLA.

Our interferometric CCS  $J_N = 4_3 - 3_2$  observations show three sub-cores, TUKH122-c1, c2, and c3 (Figure 5). Table 3 lists them. These emission peaks coincide well with the single-dish CCS  $J_N = 7_6 - 6_5$  peaks in Tatematsu et al. (2014): TUKH122-c1 roughly corresponds to their TUKH122B, and TUKH-c2 and -c3 correspond to their TUKH122. The sum of the TUKH122-c1, c2, and c3 flux is  $209 \text{ mJy km s}^{-1}$ . The single-dish observations toward TUKH122 (Tatematsu et al. 2010) show that the CCS  $J_N = 4_3 - 3_2$  intensity and linewidth are  $T_A^* = 0.47 \text{ K}$  or  $T_R = 0.78 \text{ K}$  and an FWHM linewidth of  $0.55 \text{ km s}^{-1}$ , respectively, resulting in an integrated intensity of  $0.4 \text{ K km s}^{-1}$ . This corresponds to  $1.0 \text{ Jy km s}^{-1}$  in their  $38''.5$  beam. Our interferometric observations resolved 21% of the emission. The CCS emission was detected in two velocity bins ( $2 \times 0.2 \text{ km s}^{-1}$ ) in the VLA observations. It is hard to measure the linewidth, but it will be  $\sim 0.4 \text{ km s}^{-1}$  or less. The single-dish CCS observations (Tatematsu et al. 2014) also show the emission at R.A. (J2000.0) =  $5^h 39^m 46^s.5$ , Dec. (J2000.0) =  $-7^\circ 30' 49''$  (TUKH122E), although contours are not closed due to the limited observation area. This peak is located outside the CCS observation field of the present study, but just  $30''$  southeast from the  $\text{NH}_3$  core



boundary. Then the  $\text{NH}_3$  core has the VLA CCS sub-cores on one side and the single-dish CCS on the other side, along its elongation. It is most likely that the CCS emission surrounds the  $\text{NH}_3$  core. This is very similar to the cases of cores in cold dark clouds, the  $\text{N}_2\text{H}^+$ -CCS configuration in L1544 and  $\text{NH}_3$ -CCS configuration in L1498 (Aikawa et al. 2001; Lai & Crutcher 2000). L1544 is a dense prestellar core exhibiting infall motions (Tafalla et al. 1998). Aikawa et al. (2001) calculated numerical chemical models for a collapsing core, and found that models are consistent with the observations of L1544: the collapsing core has a chemically evolved  $\text{N}_2\text{H}^+$  inner core surrounded by the chemically young CCS region. This likely also explains the  $\text{NH}_3$  and CCS configuration in TUKH122. TUKH122-n, L1544, and L1498 have similar linear sizes in pc. We wonder about the current status of TUKH122-n regarding the core stability. From the similarity between TUKH122-n and L1544, it is possible that TUKH122-n may be unstable now, or may become unstable in near future by dissipating the remaining nonthermal motion or by accreting surrounding gas after turbulence dissipation. Taking also into account high  $N(\text{N}_2\text{H}^+)/N(\text{CCS})$  ratio implying an evolved starless core (Tatematsu et al. 2014), it is most likely that TUKH122-n is a thermal starless core on the verge of star formation.

Our velocity resolution of  $0.197 \text{ km s}^{-1}$  is insufficient to allow us to see whether TUKH122 is collapsing (Zhou et al. 1993; Zhou 1995; Choi et al. 1995; Tafalla et al. 1998) or has other systematic motion such as oscillation (Lada et al. 2003; Keto & Burkert 2014; Chitsazzadeh et al. 2014). In the single-dish  $\text{N}_2\text{H}^+$  spectra of Tatematsu et al. (2014) at a resolution of  $0.1 \text{ km s}^{-1}$  toward TUKH122, there is no hint of the blue-skewed spectrum of protostellar collapse. However, it is highly desirable to obtain better velocity resolution data to investigate whether TUKH122 is collapsing or has other systematic motions.

### 3.2. TUKH083 map

Figure 6 shows the  $\text{NH}_3$  map toward TUKH083. The emission is very clumpy. Table 3 lists 5  $\text{NH}_3$  sub-cores TUKH083-n1 to n5. A feature at R.A. (J2000.0) =  $5^h36^m50^s.5$ , Dec. (J2000.0) =  $-6^\circ31'47''$  is located near the edge of the primary beam, and is as compact as the synthesized beam. Because its intensity is close to  $3\sigma$ , we do not catalog it as reliable detection. The overall complicated shape may suggest that the core is not dynamically relaxed yet. We did not detect the CCS emission toward TUKH083, although this source is the second most intense CCS  $J_N = 4_3 - 3_2$  core in Tatematsu et al. (2010). The  $3\sigma$  upper limit at  $0.4 \text{ km s}^{-1}$  resolution is  $3.6 \text{ mJy beam}^{-1} \text{ km s}^{-1}$ . This means that the CCS  $J_N = 4_3 - 3_2$  emission toward TUKH083 is extended and resolved out in our interferometric observations.

### 3.3. $\text{NH}_3$ spectra

Figures 7 and 8 show the  $\text{NH}_3$  spectra toward TUK122 and TUKH083, respectively. See Myers & Benson (1983) for details of the hyperfine components of  $\text{NH}_3$  (1, 1) and their feature names (features 1 to 8).  $\text{NH}_3$  hyperfine feature 1 is located outside our effective spectral window.  $\text{NH}_3$  hyperfine feature 4 is the main component and the other features are satellite components. The intrinsic relative intensity of hyperfine components is 0.52, 0.38, 0.56, 0.33, 0.48, and 0.28 for satellite features 2, 3, 5, 6, 7, and 8 with respect to the main component feature 4, respectively (Rydbeck et al. 1977; Ho & Townes 1983). Figure 7 shows the hyperfine component intensities toward TUKH122. Hyperfine fitting tells us that the optical depth of the main component is derived to be as large as 2. This is in contrast with the  $\text{NH}_3$  (1, 1) spectrum obtained toward the dark cloud core L1498 by Myers & Benson (1983), which looks optically thinner. TUKH083 (Figure 8) shows only  $\text{NH}_3$  hyperfine features 4 and 5, and their observed intensity ratio is close to the intrinsic

relative intensity ratio. Then, even the main component is optically thin.

### 3.4. Velocity structure in $\text{NH}_3$

Figures 9 and 10 show the intensity-weighted radial velocity maps toward TUKH122 and TUKH083, respectively. The radial velocity in TUKH122 is fairly constant over the core. We investigate the velocity field toward TUKH122-n in  $\text{NH}_3$  in detail. To see the velocity structure along the elongation, we rotate the image data anticlockwise by  $33^\circ 3'$  so that the elongation becomes vertical. Then, we average the data along the x axis (perpendicular to the elongation), and obtain the position-velocity diagram. Figure 11 illustrates the position-velocity diagram of  $\text{NH}_3$  hyperfine features 7 and 8 toward TUKH122. If all the hyperfine components are optically thin, we expect to see spatial components aligned parallel (horizontally) with each other. These hyperfine components do not show such correspondence well. Then, the optical depth probably affects the intensity distribution in these position-velocity diagrams. We derive the linewidth by using optically thinner line,  $\text{NH}_3$  hyperfine feature 8. By fitting a two-dimensional Gaussian to the  $\text{NH}_3$  hyperfine feature 8 in Figure 11, we obtain an FWHM linewidth of  $0.280 \pm 0.002 \text{ km s}^{-1}$ . Deconvolved with an instrumental velocity resolution of  $0.197 \text{ km s}^{-1}$ , the intrinsic FWHM linewidth is  $0.20 \text{ km s}^{-1}$ . This value is close to the thermal FWHM linewidth  $\Delta v(\text{th}) = (8(\ln 2)kT_k/m)^{1/2}$  for  $\text{NH}_3$  at  $T_k = 10 \text{ K}$  of  $0.16 \text{ km s}^{-1}$ . Here,  $k$  is the Boltzmann constant, and  $m$  is the mass of the molecule. The FWHM linewidth for the mean mass per particle (2.33 a.m.u.) at 10 K is  $0.44 \text{ km s}^{-1}$ . The turbulent FWHM linewidth  $\Delta v(\text{turb})$  and total FWHM linewidth  $\Delta v(\text{tot})$  (Myers & Benson 1983) are derived to be 0.16 and  $0.47 \text{ km s}^{-1}$ , respectively. Because  $\Delta v(\text{th}) > \Delta v(\text{turb})$ , TUKH122-n is thermally dominated. If there is a velocity gradient across (perpendicular to) the elongation, it may contribute to  $\Delta v(\text{turb})$ , but we do not see any hint of such a gradient across the elongation. We observe

a slight velocity gradient of  $3.6 \text{ km s}^{-1} \text{ pc}^{-1}$  along the elongation from feature 8 in Figure 11. Then, the specific angular momentum  $J/M = (2/5)Rv_{rot}$  ( $2/5$  for a sphere) is  $1.2 \times 10^{-3} \text{ km s}^{-1} \text{ pc}$ . This follows the empirical best-fit  $J/M - R$  relationship obtained by Goodman et al. (1993) for  $R = 0.03\text{--}0.3 \text{ pc}$ , or is located slightly lower (smaller  $J/M$ ). We derive the ratio  $\beta$  of rotational energy to the gravitational energy. We adopt the definition of  $\beta = (1/3) \omega^2 R^3 / GM$  (Goodman et al. 1993), and obtain  $\beta = 1.6 \times 10^{-2}$ . Here,  $\omega$  is the angular speed, and  $G$  is the gravitational constant. This small value ( $\ll$  unity) is close to the typical value of 0.02 obtained in dark cloud cores (Goodman et al. 1993), and indicates that the core is not rotationally supported. Because the axial ratio of the core TUKH122-n is as small as 0.26 and rotation cannot account for core elongation, it is likely that magnetic fields play a key role in the core shaping of TUKH122. Nakano (1998) has concluded that molecular clouds are magnetically supercritical. Crutcher (1999) has shown that the mass-to-magnetic flux ratio is about twice as critical, and static magnetic fields and turbulence (MHD waves) are equally important in cloud energetics. He has concluded that magnetic fields are important in the physics of molecular clouds. Our observations seem to be consistent with his conclusion.

Next, we look into the case of TUKH083. Figure 12 shows the position-velocity diagram along right ascension toward TUKH083 of  $\text{NH}_3$  hyperfine feature 4. The emission is integrated along declination within a box containing the detected  $\text{NH}_3$  emission. Precisely, feature 4 consists of eight hyperfine components, and the two most intense components have a frequency difference corresponding to  $0.32 \text{ km s}^{-1}$  (Rydbeck et al. 1977). However, for the TUKH083  $\text{NH}_3$  core, it is hard to separate hyperfine components in feature 4 because of overcrowding.

### 3.5. Comparison between TUKH122, TUKH 123, and the dark cloud core L1544

We compare the physical parameters of our cores in Orion and the dark cloud core L1544 in Taurus. To the east of TUKH122, a cluster-forming core TUKH123 accompanying L1641-south3 (Fukui 1989) containing six protostars (Megeath et al. 2012) is located (Figure 2). Table 4 summarizes the physical parameters of TUKH122 and TUKH123 in the Orion A GMC, and that of L1544 in the dark cloud. The CS  $J = 1-0$  data of TUKH122, and TUKH123 are taken from Tatematsu et al. (1993), and the data of L1544 is taken from Benson & Myers (1989); Tafalla et al. (1998). We adopt the  $\text{NH}_3$  rotation temperature for Orion cores from Wilson et al. (1999), and converted it to the kinetic temperature  $T_k$  using the relation given by Danby et al. (1988). For TUKH122 and TUKH123, Wilson et al. (1999) list upper limits of  $T_k < 15$  K, and we adopted  $T_k = 10$  K assuming that they have temperatures similar to those in cores in cold dark clouds. Regarding the radius  $R$ , we adopt the HWHM (= FWHM/2) radius. The major and minor radius at the half-maximum level are deconvolved values for the synthesized beam. Then, the radius  $R$  is calculated from a geometrical mean of the major and minor radius. Regarding linewidth, we adopt the definition of the total linewidth  $\Delta v$  (tot) from Myers (1983), which takes into account the difference between the mass of the observed molecule and the mean mass per particle. We use the virial mass instead of the LTE mass here, because the molecular abundance is not precisely known. The virial mass is derived by using the total linewidth instead of the observed linewidth, and therefore is slightly different from those reported in Tatematsu et al. (1993) and Tafalla et al. (1998). The gas density is derived from the radius and virial mass, and defined as  $n = 1.2 n(\text{H}_2)$  by taking into account the contribution of He. We list the free-fall time estimated from density. Table 4 shows that TUKH122-n in  $\text{NH}_3$  and L1544 in  $\text{N}_2\text{H}^+$  are very similar in the kinetic temperature (10 K), linear size (0.03 pc radius), and mass ( $\sim 2 M_\odot$ ). It was often suggested that cores in GMCs and

those in cold dark clouds are different in the physical properties (e.g. Turner 1988), but our observations revealed that the Orion A GMC contains at least one core very similar to the dark cloud core.

## 4. Discussion

### 4.1. Turbulence in cores

The  $\text{NH}_3$  cores of TUKH083 and TUKH122 are embedded in the CS core observed by Tatematsu et al. (1993). The thermal Jeans length and mass of the CS core are calculated for the adopted kinetic temperature  $T_k$  (table 3). The virial mass of the TUKH122-n core  $1.5 M_\odot$  is close to the Jeans mass in the parent turbulent CS core. This is consistent with an idea that TUKH122-n has been formed as gravitational instability in the parent turbulent equilibrium core.

The intrinsic  $\text{NH}_3$  linewidth in our interferometric observations is as small as  $0.20 \text{ km s}^{-1}$ . The single-dish CCS  $J_N = 7_6 - 6_5$  and  $\text{N}_2\text{H}^+$  linewidth are  $0.27\text{--}0.39$  and  $0.27\text{--}0.28 \text{ km s}^{-1}$ , respectively (Tatematsu et al. 2014), and are almost thermal. On the other hand, the single-dish CS  $J = 1\text{--}0$  linewidth toward TUKH122 is as large as  $0.83 \text{ km s}^{-1}$  (Tatematsu et al. 1993). According to Tatematsu et al. (1998) the optical depth of this line is  $< 0.9$ , and therefore the linewidth will not be seriously affected. Figure 13 shows the CS  $J = 1\text{--}0$  velocity channel map of Tatematsu et al. (1993) toward TUKH122. The CS emission is centered at the field center of the  $\text{NH}_3$  and CCS observations, from  $v_{LSR-K} = 3.6$  to  $4.2 \text{ km s}^{-1}$ . Then, it is observed as a non-thermal, turbulent core. In our observations, the CCS emission is observed only within a range of  $0.4 \text{ km s}^{-1}$  toward TUKH122, which is close to the thermal FWHM linewidth. These facts will imply turbulence dissipation in TUKH122: the turbulent TUKH122 CS core ( $R = 0.18 \text{ pc}$ ,  $\Delta v(\text{tot}) = 0.94 \text{ km s}^{-1}$ ) has formed the

quiescent, thermal  $\text{NH}_3$  core associated with CCS inside. The viral mass and corresponding column density of the TUKH122 CS core is  $33 M_\odot$  and  $N(\text{H}_2) = 2.2 \times 10^{21} \text{ cm}^{-2}$ , respectively. This column density is consistent with that obtained from dust continuum observations with the Herschel Observatory (Roy et al. 2013),  $N(\text{H}_2) = 1.6\text{--}1.9 \times 10^{21} \text{ cm}^{-2}$  from their figure. Furthermore, the  $\text{NH}_3$  core looks dynamically relaxed, reminding us of quasistatic evolution. The  $\text{NH}_3$  and CS cores are located in the CS filament (Figure 2). We suggest that the turbulent equilibrium CS cores are formed from the turbulent filamentary molecular cloud due to the gravitational instability (Hanawa et al. 1993), and the dynamically relaxed thermal  $\text{NH}_3$  cores are then formed slowly with turbulence dissipation and gravitational instability.

Although the TUKH122 and L1544  $\text{NH}_3$  cores are very similar in terms of the kinetic temperature, linear size, and mass, they differ in terms of the mass of parent core: TUKH122 has a turbulent massive ( $\sim 30 M_\odot$ ) parent core observed, while L1544 has a thermal less-massive ( $\sim 10 M_\odot$ ) parent core. Indeed, it is known that 0.1 pc-sized cores in the Orion A GMC have systematically larger linewidths and larger masses than similar-size cores in cold dark clouds (Tatematsu et al. 1993). It is possible that such a difference is related to an ability for GMC cores to form star clusters. In dark cloud cores, Goodman et al. (1998); Lai & Crutcher (2000) investigated the single-tracer single-cloud linewidth-size relation, and concluded that linewidth becomes coherent (thermal-motion dominated constant values against radius) on length scales less than  $\sim 0.1$  pc. Pineda et al. (2010) concluded that a transition to coherence occurs at 0.04 pc at B5 in the Perseus cold dark cloud. GMC cores have different linewidth-size relation compared with dark cloud cores Tatematsu et al. (1993); Caselli & Myers (1995). Judging from Figure 6 of Caselli & Myers (1995), the transition in GMC cores may occur at a smaller radius (0.01–0.1 pc). This is consistent with our observations.

#### 4.2. Comparison between TUKH083 and TUKH122

We found that TUKH083 and TUKH122 are very different in the distribution of the  $\text{NH}_3$  emission. TUKH083 is clumpy, while TUKH122 has a smooth oval boundary. In CCS, TUKH122 was detected in the interferometric observations, but TUKH083 was not detected. This means that the CCS emission distribution is more compact in TUKH122 than in TUKH083. There are two possibilities. First, because TUKH083 is warmer than TUKH122, different temperatures caused different core formation modes. Second, TUKH083 is younger, and has not been dynamically relaxed yet. From  $N(\text{NH}_3)/N(\text{CCS})$  and  $N(\text{N}_2\text{H}^+)/N(\text{CCS})$  (Tatematsu et al. 2010, 2014), TUKH083 is most likely younger than TUKH122. However, clearly we need more samples to establish the picture of core evolution in various environments in GMCs.

### 5. Summary

We mapped two starless molecular cloud cores, TUKH083 and TUKH122, in the Orion A GMC in CCS and  $\text{NH}_3$  with the VLA. The TUKH122  $\text{NH}_3$  core (TUKH122-n) is elongated, and has a smooth oval boundary. Where observed, the CCS emission surrounds the  $\text{NH}_3$  core. This is very similar to  $\text{N}_2\text{H}^+$ -CCS distribution in the Taurus cores L1544 and L1498. TUKH122-n has an  $\text{NH}_3$  linewidth of  $0.20 \text{ km s}^{-1}$ , which implies that the core is thermally supported. The linewidth and shape of the  $\text{NH}_3$  core seem to represent a dynamically relaxed quiescent core. TUKH122-n (associated with CCS) is embedded in the parent turbulent CS core, which suggests TUKH122-n has formed through turbulence dissipation. The parent core of TUKH122-n is three times more massive than that of L1544, which may suggest difference in the capability of forming the cluster. The physical parameters of TUKH122-n resemble those of the L1544  $\text{NH}_3$  core. The virial mass of the TUKH122-n core is  $1.5 M_\odot$ , and is on the order of the Jeans mass of the parent CS core.



TUKH083 was detected in  $\text{NH}_3$  showing complicated distribution, but not in CCS. The CCS emission toward TUKH083 appears to be resolved out.

K.T. is grateful to Tomoyuki Hanawa for comments on the draft. The authors would like to thank an anonymous referee for helpful comments. Data analysis were carried out on the common use data analysis computer system at the Astronomy Data Center, ADC, of the National Astronomical Observatory of Japan. M.C. was supported by the Core Research Program of National Research Foundation funded by the Ministry of Science, ICT and Future Planning of the Korean government (grant number NRF-2011-0015816). J.-E.L. was supported by the Basic Science Research Program through the National Research Foundation of Korea (NRF) funded by the Ministry of Education of the Korean government (grant number NRF-2012R1A1A2044689).

*Facility:* VLA.

## REFERENCES

- Aikawa Y., Ohashi, N., Inutsuka, S., Herbst, E., & Takakuwa, S. 2001, *ApJ*, 552, 639
- Aso, Y., Tatematsu, K., Sekimoto, Y., Nakano, T., Umemoto, T., Koyama, K., & Yamamoto, S. 2000, *ApJS*, 131, 465
- Bally, J., Langer, W.D., Stark, A.A., & Wilson, R.W. 1987, *ApJ*, 312, L45
- Ballesteros-Paredes, J., Klessen, R. S., & Vázquez-Semadeni, E. 2003, *ApJ* 592, 188
- Ballesteros-Paredes, J., Klessen, R. S., Mac Low, M.-M., & Vázquez-Semadeni, E. 2007, *Protostars and Planets V*, B. Reipurth, D. Jewitt, and K. Keil (eds.) (Tucson: University of Arizona Press), 63
- Batrla, W., Wilson, T.L., Bastien, P. & Ruf, K. 1983, *A&A*, 128, 279
- Benson, P.J. & Myers, P.C. 1989, *ApJS*, 71, 89
- Bergin, E.A., & Tafalla, M. 2007, *ARA&A*, 45, 339
- Caselli, P., & Myers, P.C. 1995, *ApJ*, 446, 665
- Castets, A., Duvert, G., Dutrey, A., Bally, J., Langer, W.D., & Wilson, R.W. 1990, *A&A*, 234, 469
- Cesaroni, R., & Wilson, T.L. 1994, *A&A*, 281, 209
- Chitsazzadeh, S., Di Francesco, J., Schnee, S., Friesen, R.K., Shimajiri, Y., Langston, G.I., Sadavoy, S.I., Keto, E.R., Pineda, J.E., Takakuwa, S., & Tatematsu, K. 2014, *ApJ*, in press
- Chini, R., et al. 1997, *ApJ*, 474, L135
- Choi, M., Evans, N.J., II, Gregersen, E.M., & Wang, Y. 1995, *ApJ*, 448, 742

- Crutcher, R.M. 1999 ApJ, 520, 706
- Danby, G., et al. 1988, MNRAS, 235, 229
- Fukui, Y., in ESO Workshop on Low Mass Star Formation and Pre-Main Sequence Objects, ed. B. Reipurth (Garching: ESO), 95
- Genzel, R., & Stutzki, R. 1989, ARA&A, 27, 41
- Goodman, A.A., Benson, P.J., Fuller, G.A., & Myers, P.C. 1993 ApJ, 406, 528
- Goodman, A.A., Barranco, J.A., Wilner, D.J., & Heyer, M.H. 1998 ApJ, 504, 223
- Hanawa, T., Nakamura, F., Matsumoto, T., Nakano, T., Tatematsu, K., Umemoto, T., et al. 1993, ApJ404, L83; Erratum, 1993, 412, L75
- Hirota, T., Ohishi, M., & Yamamoto, S. 2009, ApJ, 699, 585
- Ho, P.T.P., & Townes, C.H. 1983, ARA&A, 21, 239
- Ikeda, N., Sunada, K., & Kitamura, Y. 2007, ApJ, 665, 1194
- Johnstone, D., & Bally, J. 1999, ApJ, 510, L49
- Johnstone, D., & Bally, J. 2006, ApJ, 653, 383
- Keto, E., & Burkert, A. 2014, MNRAS, 441,1468
- Kim, M.K., et al. 2008, PASJ, 60, 991
- Lada, C.J., Bergin, E.A., Alves, J.F., Huard, T.L. 2003, ApJ, 586, 286
- Lai, S.-P., & Crutcher, R.M. 2000, ApJS, 128, 271
- Lis, D.C., Serabyn, E., Dowell, C.D., Benford, D.J., Phillips, T.G., Hunter, T.R., & Wang, N. 1998, ApJ, 509, 299

- Lombardi, M., Bouy, H., Alves, J., & Lada, C.J. 2014, A&A, in press
- Megeath, S.T., et al. 2012, ApJ, 144, 192
- Myers, P.C., & Benson, P.J. 1983, ApJ, 266, 309
- Myers, P.C. 1983, ApJ, 270, 105
- Myers, P.C., Fuller, G.A., Goodman, A.A., & Benson, P.J. 1991, ApJ, 376, 561
- Nagahama, T., Mizuno, A., Ogawa, H., & Fukui, Y. 1998, ApJ, 116, 336
- Nakano, T. 1998, ApJ, 494, 587
- Pineda, J.E., Goodman, A.A., Arce, H.G., Caselli, P., Foster, J.B., Myers, P.C., & Rosolowsky, E.W. 2010, ApJ, 712, L116
- Pineda, J.E., Goodman, A.A., Arce, H.G., Caselli, P., Longmore, S., & Corder, S. 2011, ApJ, 739, L2
- Roy, A., Martin, P.G., Polychroni, D., Bontemps, S., Abergel, A., André, P., et al. 2013, ApJ, 763, 55
- Rydbeck, O.E.H, Sume, A., Hjalmarson, Å, Elldér, J., Rönnäng, B.O., & Kollberg, E. 1977, ApJ, 215, L35
- Shu, F.H., Adams, F.C., & Lizano, S. 1987, ARA&A, 25, 23
- Suzuki, H., Yamamoto, S., Ohishi, M., Kaifu, N., Ishikawa, S.-I., Hirahara, Y., & Takano, S. 1992, ApJ, 392, 551
- Tafalla, M., Mardones, D., Myers, P.C., Caselli, P., Bachiller, R. & Benson, P.J. 1998 ApJ, 504, 900
- Takahashi, S., Ho, P.T.P, Teixeira, P.S., Zapata, L.A., & Su, Y.-N. 2013, ApJ, 763, 57

- Tatematsu, K., et al. 1993, *ApJ*, 404, 643
- Tatematsu, K., Umemoto, T., Heyer, M. H., Hirano, N., Kameya, O., & Jaffe, D. T. 1998, *ApJS*, 118, 517
- Tatematsu, K., Kandori, R., Umemoto, T., & Sekimoto, Y. 2008, *PASJ*, 60, 407
- Tatematsu, K., Hirota, T., Kandori, R., & Umemoto, T. 2010, *PASJ*, 62, 1473
- Tatematsu, K., Ohashi, S., Umemoto, T., Lee, J.-E., Hirota, T., Yamamoto, S., et al. 2014, *PASJ*, 66, 16
- Turner, B.E. 1988, in *Galactic and Extragalactic Radio Astronomy*, ed. G.L. Verschuur & K.I. Kellermann (2d ed.; New York: Springer-Verlag), 154
- Wilson, T.L., Mauersberger, R., Gensheimer, P.D., Muters, D., & Bieging, J.H. 1999, *ApJ*, 525, 343
- Yamamoto, S, Saito, S., Kawaguchi, K., Chikada, Y., Suzuki, H., Kaifu, N., Ishikawa, S. & Ohishi, M. 1990, *ApJ*, 361, 318
- Zhou, S., Evans, N.J., II, Kümpe, C. & Walmsley, C.M. 1993, *ApJ*, 404, 232
- Zhou, S. 1995, *ApJ*, 442, 685

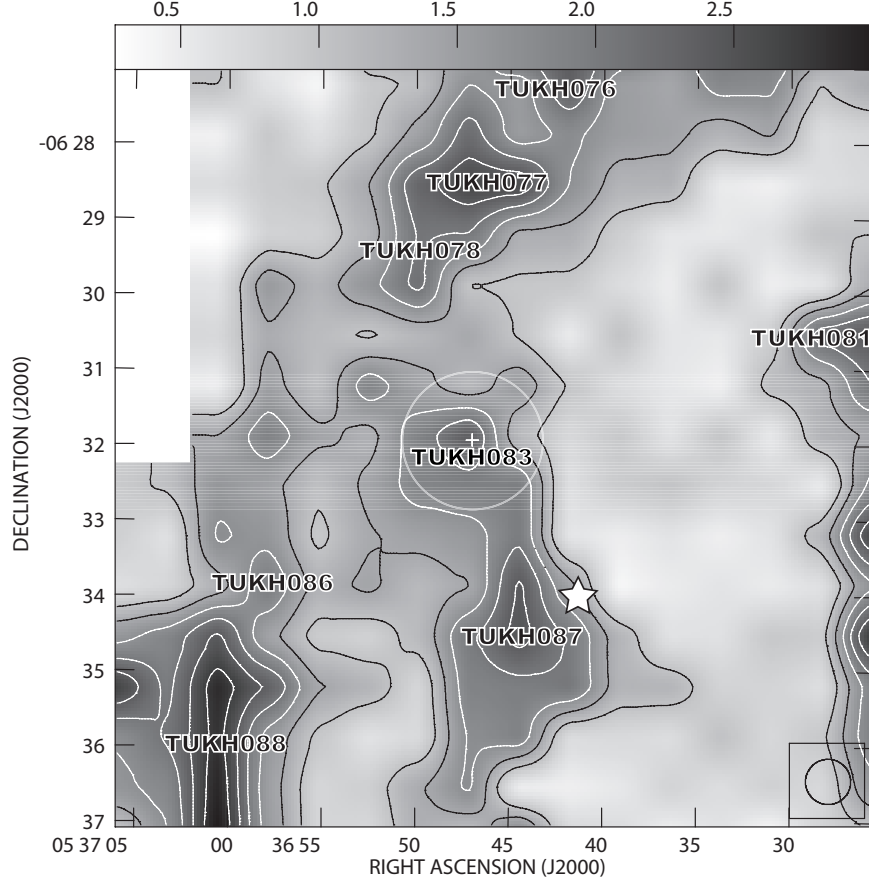


Fig. 1.— CS  $J = 1-0$  peak intensity map around TUKH083 taken from Tatematsu et al. (1993). The contour starts at  $3\sigma$  with an interval of  $1\sigma$ , where  $1\sigma$  is  $T_A^* = 0.34$  K or the main-beam radiation temperature  $T_R = 0.57$  K. The position of the Spitzer protostar (Megeath et al. 2012) is shown with the star sign. The primary beam (field of view) of the VLA observations at K band is shown as a white circle centered at the plus sign. The

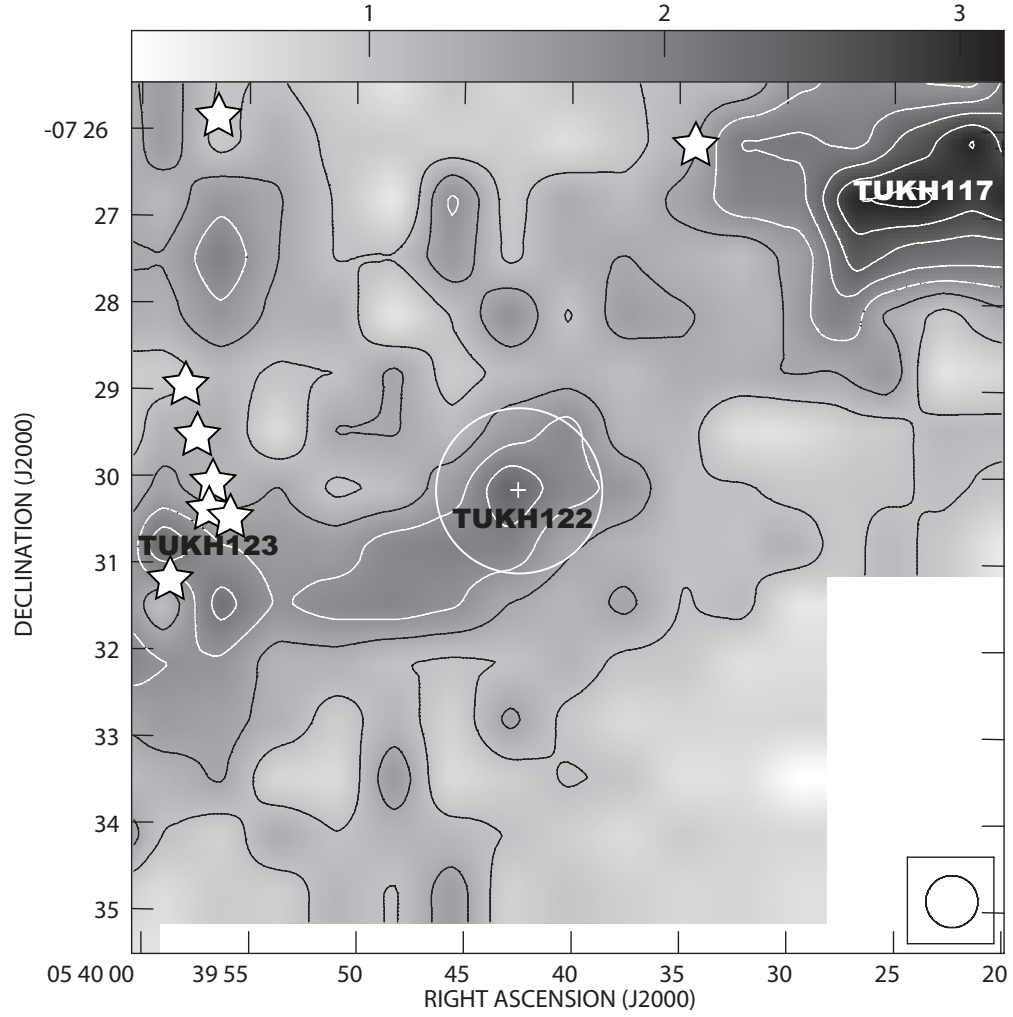


Fig. 2.— The same as Figure 1 but for TUKH122. The cluster of Spitzer sources associated with core TUKH123 is L1641-south3 (Fukui 1989).

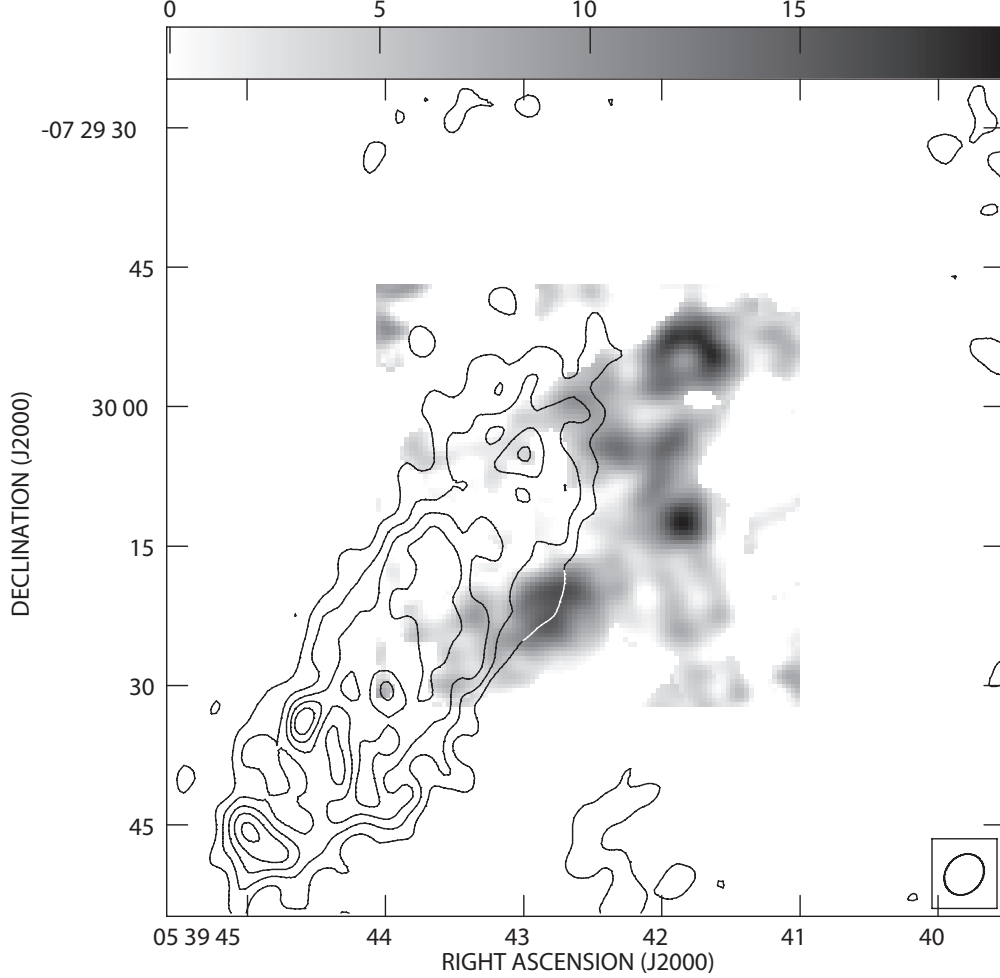


Fig. 3.— CCS integrated intensity map (gray scale) superimposed on  $\text{NH}_3$  integrated intensity map (contours) toward TUKH122. The lowest contour level and contour interval are  $2.4 \text{ mJy beam}^{-1} \text{ km s}^{-1}$ . The maximum intensity for the gray scale and the contour are 19.8 and  $14.3 \text{ mJy beam}^{-1} \text{ km s}^{-1}$ , respectively. In the lower right corner, the synthesized beam for CCS is shown. That for  $\text{NH}_3$  has a similar size. The CCS emission was observed only in the central area (see Figures 4 and 5 for the detailed observed areas).



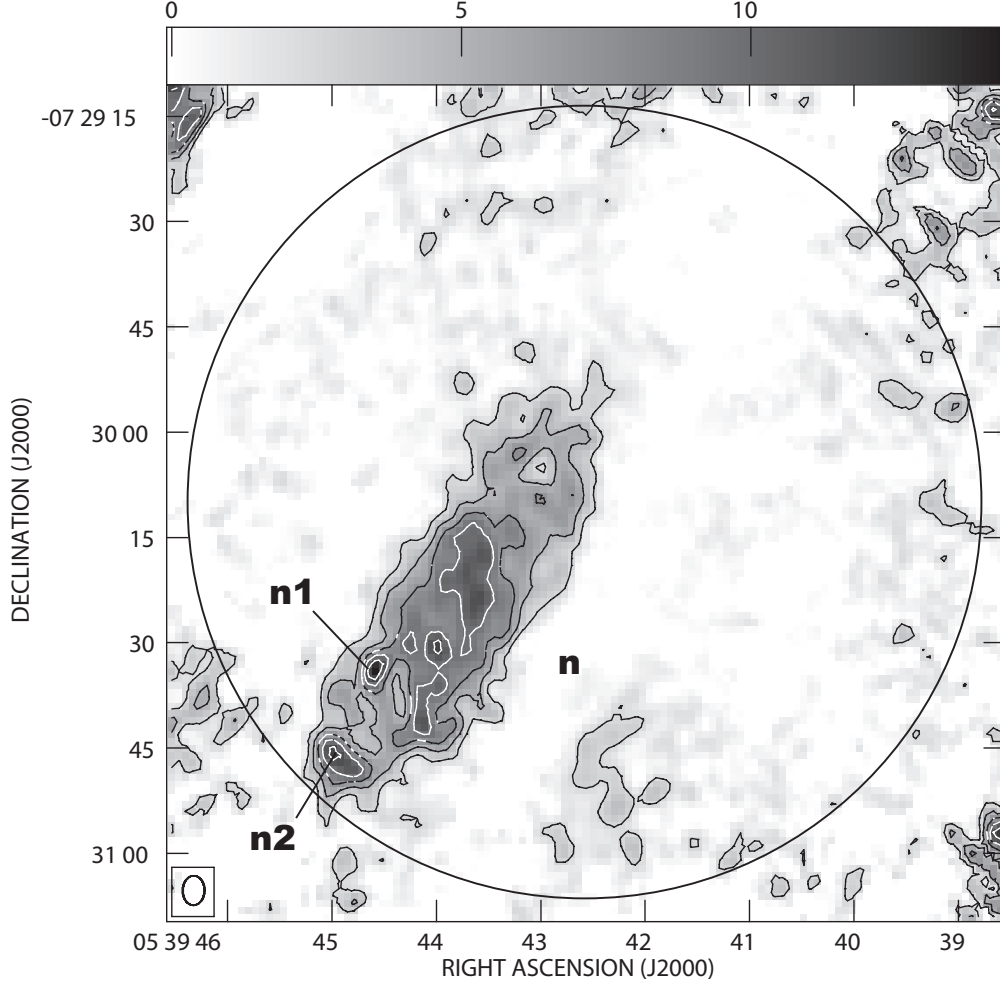


Fig. 4.—  $\text{NH}_3$  velocity-integrated intensity map of the main  $\text{NH}_3$   $(J, K) = (1, 1)$  component toward TUKH122. The velocity integration range is from  $v_{\text{LSR}-K} = 3.2$  to  $4.4 \text{ km s}^{-1}$ . The large circle delineates the primary beam of the interferometric observations. The lowest contour level and contour interval are  $2.4 \text{ mJy beam}^{-1} \text{ km s}^{-1}$ , which corresponds to  $3\sigma$  and  $1.5\sigma$  at the map center and at the edge of the primary beam, respectively. The maximum intensity in the primary beam is  $14.3 \text{ mJy beam}^{-1} \text{ km s}^{-1}$ . In the lower left corner, the synthesized beam is shown.

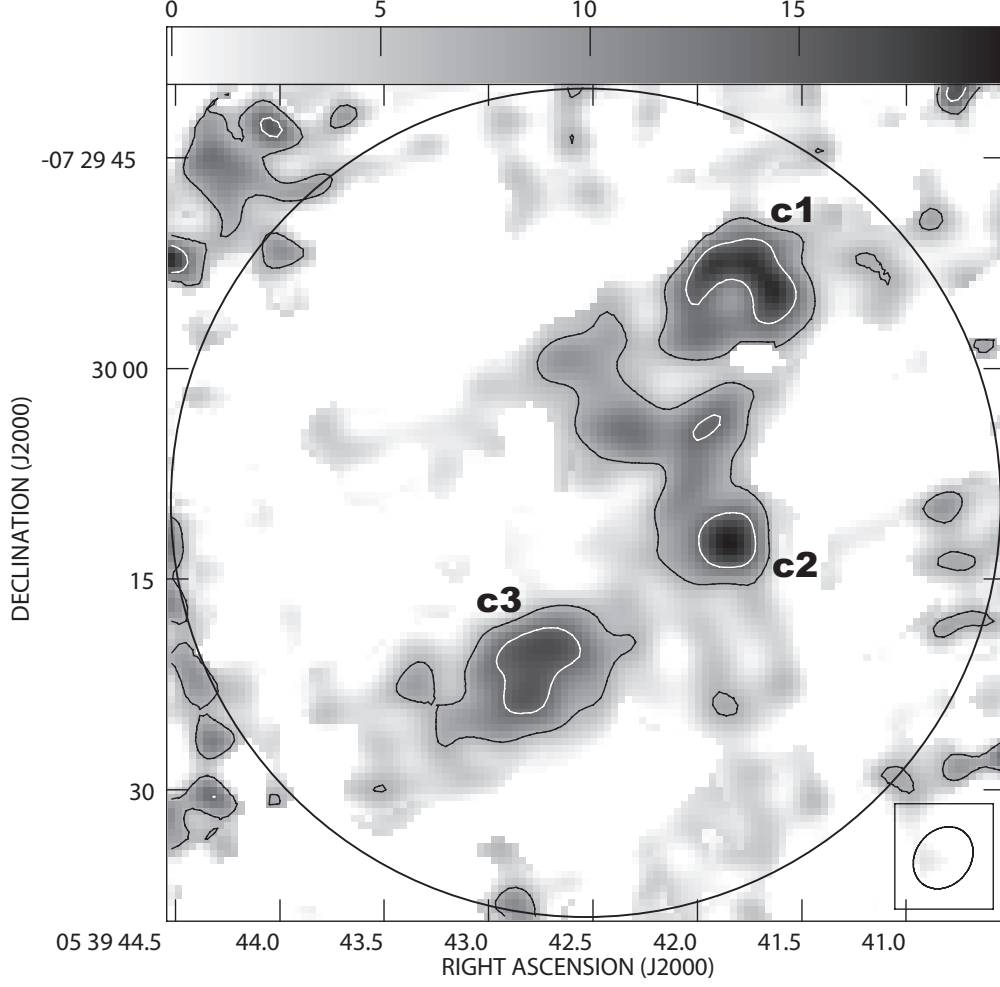


Fig. 5.— CCS velocity-integrated intensity map toward TUKH122. The velocity integration range is from  $v_{LSR-K} = 3.6$  to  $4.0 \text{ km s}^{-1}$ . The large circle delineates the primary beam size of the interferometric observations. The contour interval is  $6.9 \text{ mJy beam}^{-1} \text{ km s}^{-1}$ , which corresponds to  $3\sigma$  and  $1.5\sigma$  at the map center and at the edge of the primary beam, respectively. The maximum intensity in the primary beam is  $19.8 \text{ mJy beam}^{-1} \text{ km s}^{-1}$ . In the lower right corner, the synthesized beam is shown.

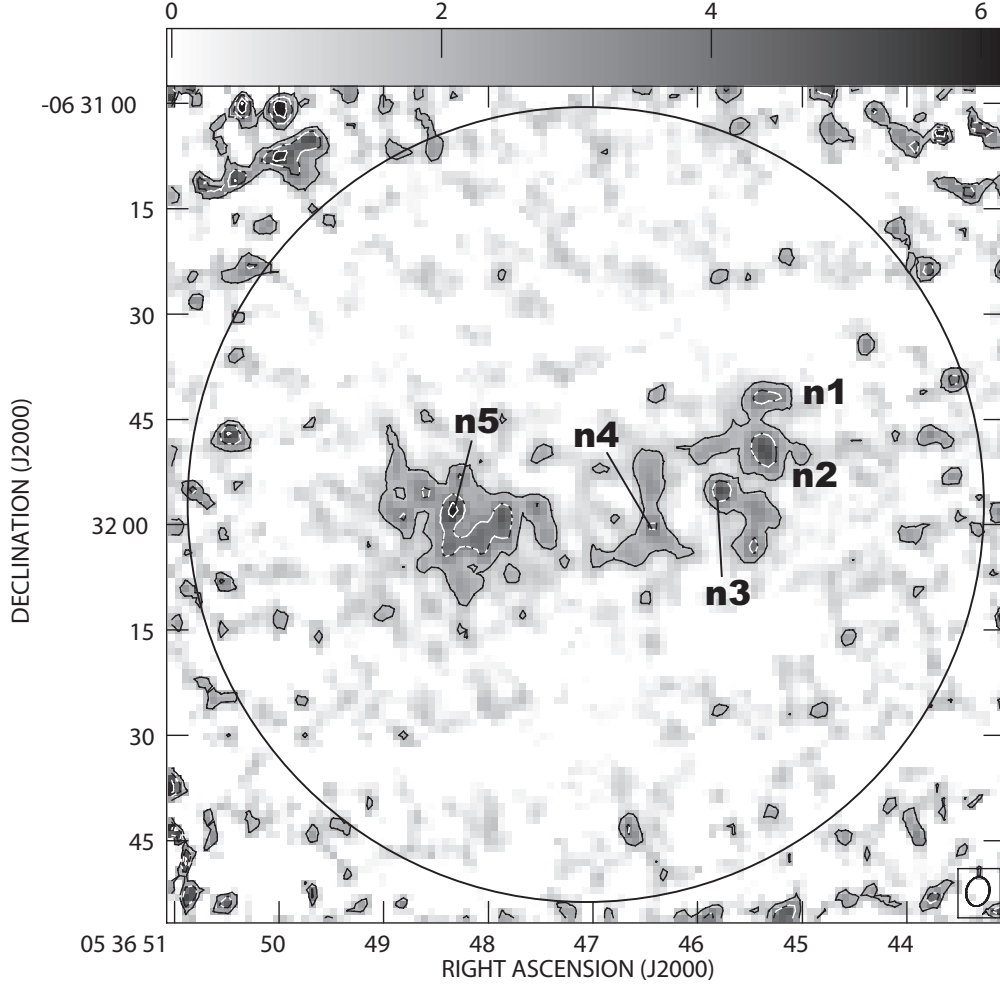


Fig. 6.— NH<sub>3</sub> integrated intensity map of the main NH<sub>3</sub> ( $J, K$ ) = (1, 1) component toward TUKH083. The velocity integration range is from  $v_{LSR-K} = 6.8$  to  $7.8$  km s<sup>-1</sup>. The contour interval is 1.8 mJy beam<sup>-1</sup> km s<sup>-1</sup>, which corresponds to  $3\sigma$  and  $1.5\sigma$  at the map center and at the edge of the primary beam, respectively. The maximum intensity in the primary beam is 6.2 mJy beam<sup>-1</sup> km s<sup>-1</sup>.

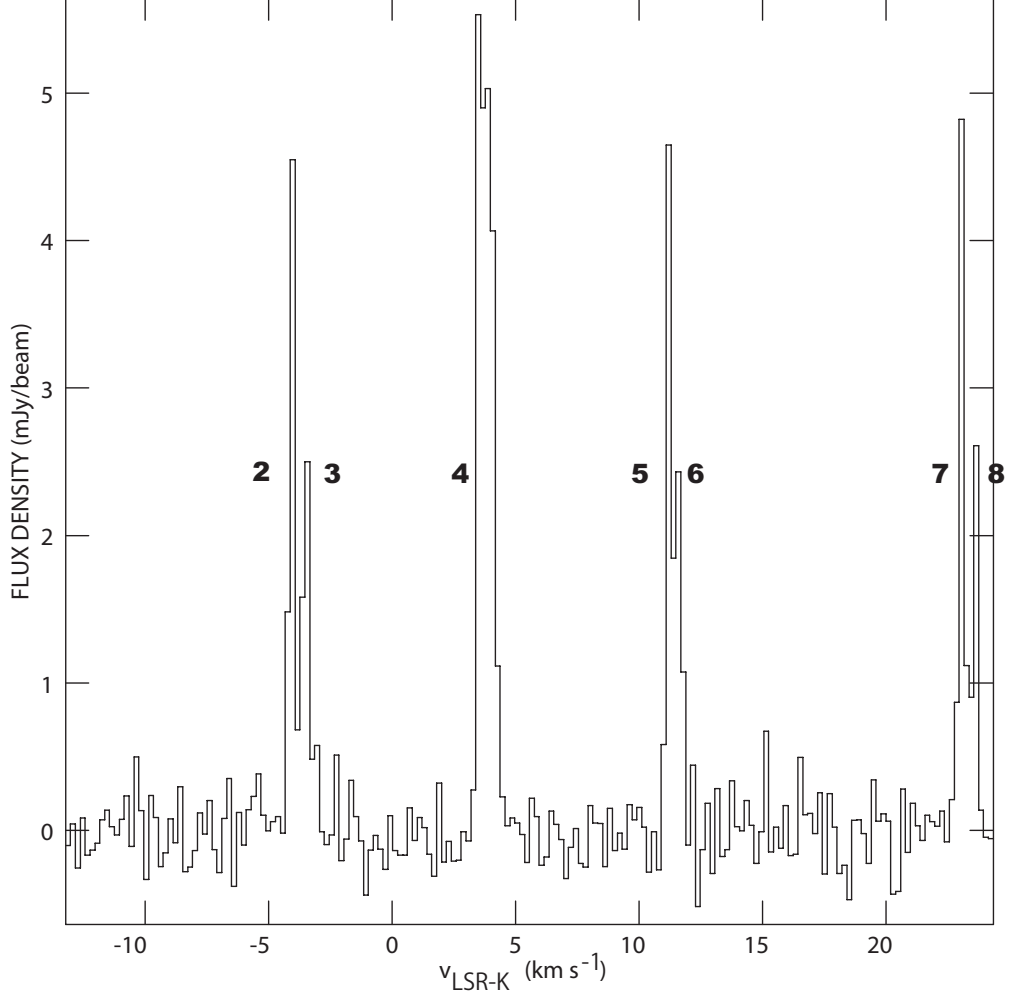


Fig. 7.—  $\text{NH}_3$  spectrum toward TUKH122. The abscissa is the LSR-K radial velocity with respect to the  $\text{NH}_3$   $(J,K) = (1,1)$  main component (feature 4). The rotated rectangle enclosing TUKH122-n is used for the average spectrum.

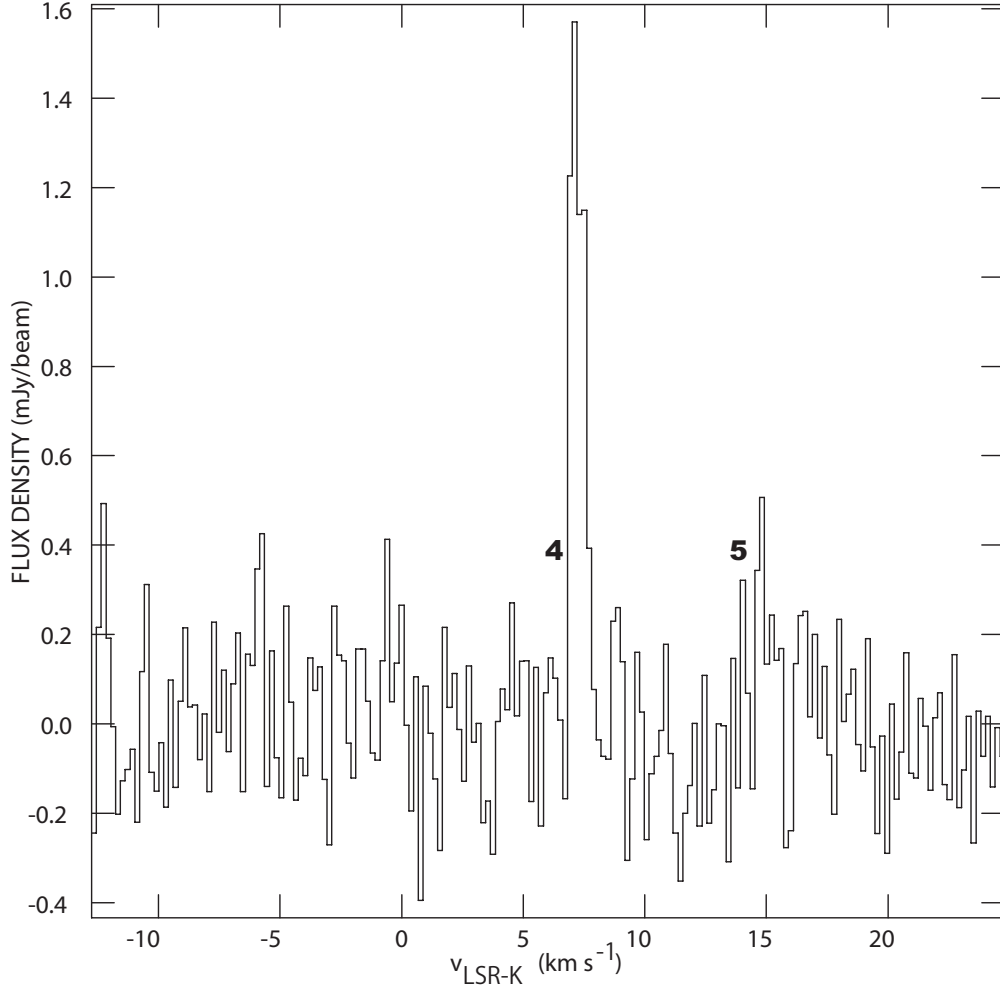


Fig. 8.— The same as Figure 7 but for TUKH083. The rectangle enclosing TUKH122-n is used for the average spectrum.  $\text{NH}_3$  hyperfine feature 1 is located outside the effective spectral window.

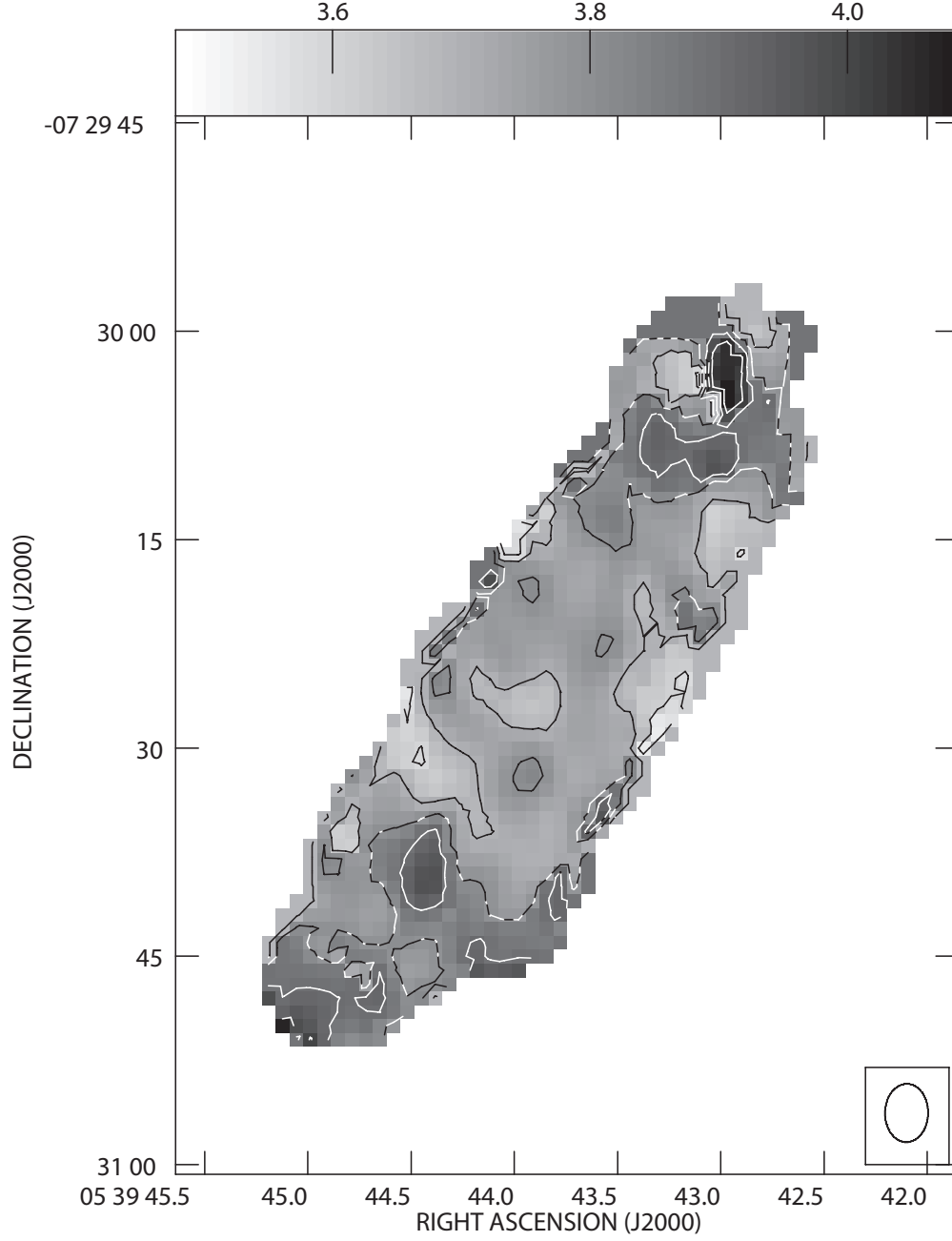


Fig. 9.—  $\text{NH}_3$  moment 1 (intensity-weighted velocity) map of the  $\text{NH}_3$  ( $J, K$ ) = (1, 1) feature 4 (main component) toward TUKH122. The unit for the velocity is  $\text{km s}^{-1}$ . Coutours are drawn at  $v_{\text{LSR}-K} = 3.6, 3.7, 3.8, 3.9,$  and  $4.0 \text{ km s}^{-1}$ . The data above  $2\sigma$  at the original channel were used for the moment 1 calculation.

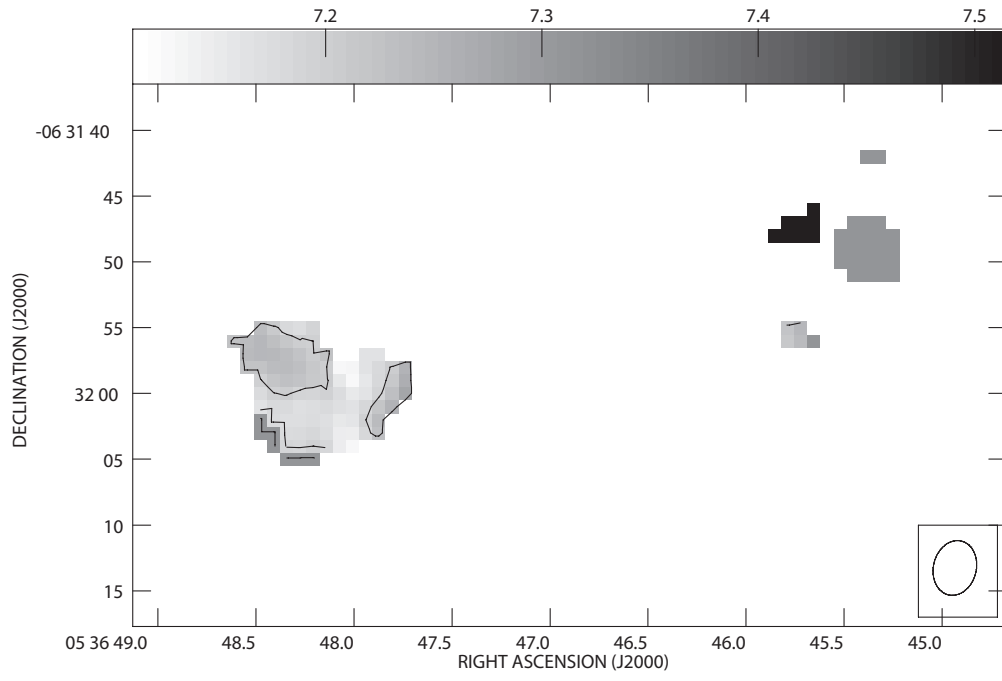


Fig. 10.— The same as Figure 9 but for TUKH083. Contours are drawn at  $v_{LSR-K} = 7.2$  and  $7.3 \text{ km s}^{-1}$ .

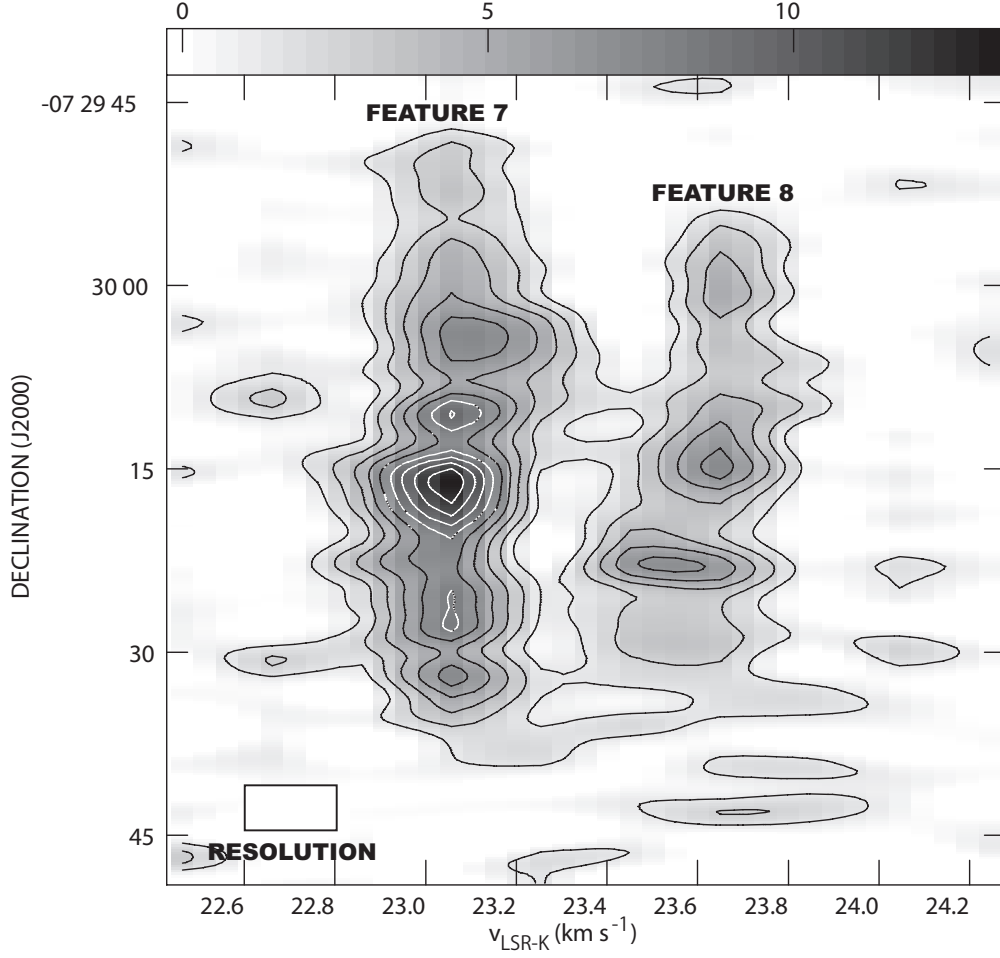


Fig. 11.— The position-velocity diagram for TUKH122 for  $\text{NH}_3$  hyperfine features 7 and 8. Contours represent 10, 20, 30, 40, 50, 60, 70, 80, and 90% of the maximum value of  $13.2 \text{ mJy beam}^{-1}$ . The position (declination) is labeled for the eastern side of the  $33.3$ -degree anticlockwisely rotated rectangle enclosing TUKH122-n. The spectra are averaged across the core elongation. The radial velocity  $v_{\text{LSR-K}}$  is labeled for the feature 4. For features 7 and 8,  $19.31$  and  $19.87 \text{ km s}^{-1}$  should be subtracted to obtain the true radial velocity, respectively.



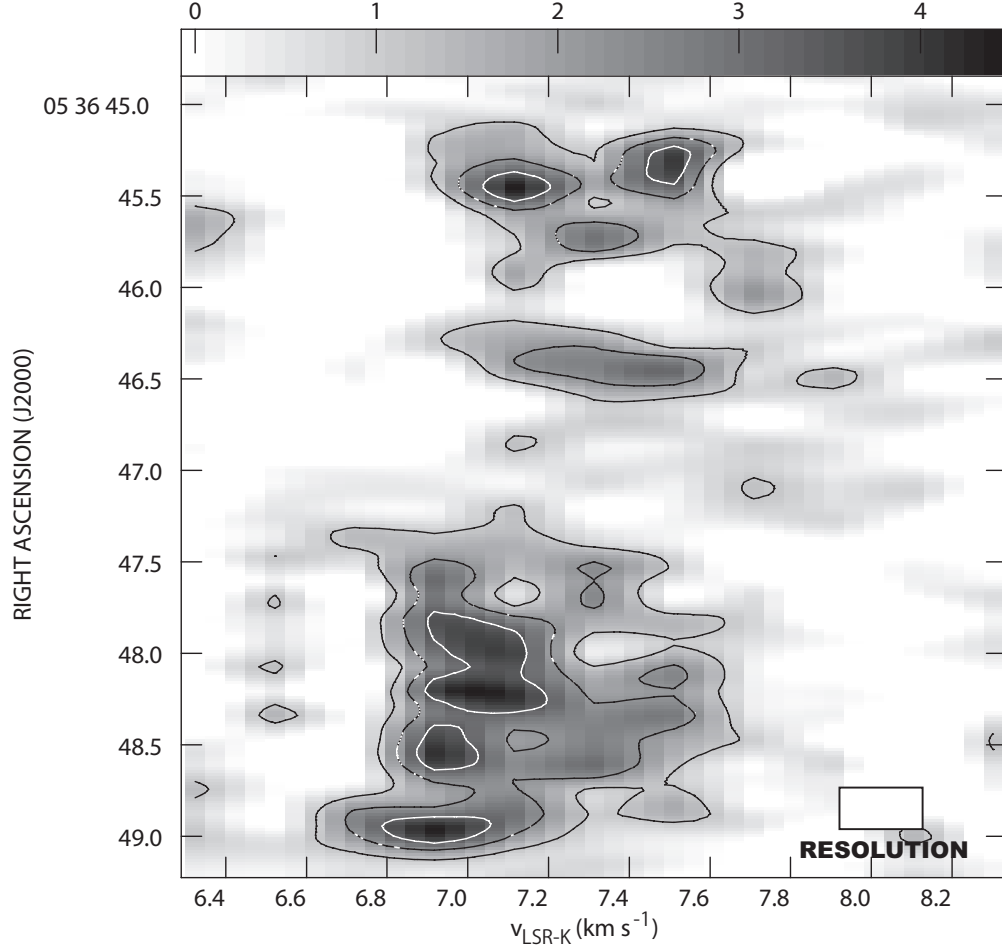


Fig. 12.—  $\text{NH}_3$  position-velocity diagram along right ascension toward TUKH083 of  $\text{NH}_3$  hyperfine feature 4. The spectra are averaged along declination within the rectangle enclosing the detected  $\text{NH}_3$  emission. Contours are drawn at 25%, 50%, and 75% with respect to the maximum value of  $4.4 \text{ mJy beam}^{-1}$ .

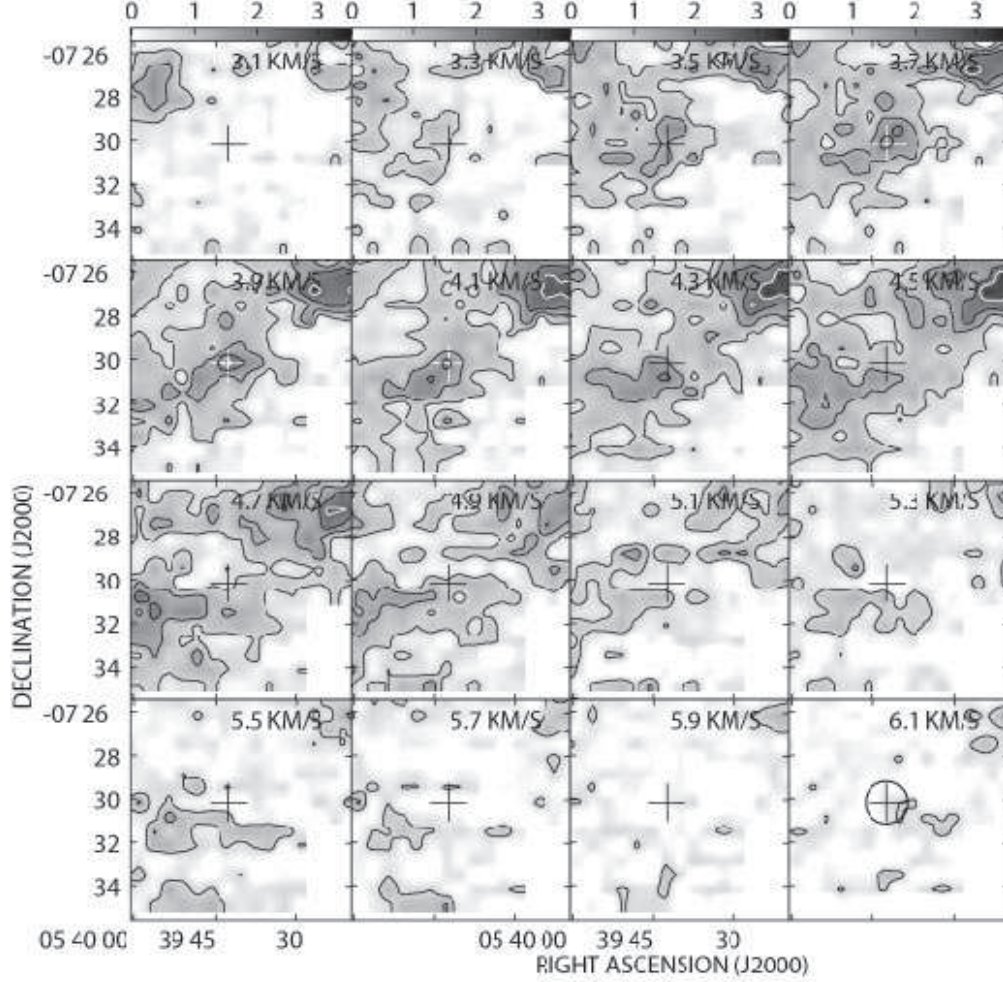


Fig. 13.— CS  $J = 1-0$  velocity channel maps of Tatematsu et al. (1993). Contours are drawn from 20% to 80% with a step of 20% with respect to the maximum value of  $T_A^* = 3.1$  K or  $T_R = 5.2$  K. The plus sign represents the center of the primary beam size of our  $\text{NH}_3$  and CCS observations. The circle at  $v_{LSR-K} = 6.1 \text{ km s}^{-1}$  represents the primary beam size (field of view) for  $\text{NH}_3$  observations.

Table 1. Observation Sessions

Date	Observation File Name	Band	Number of Usable Antennas	Used for Image?
2010 August 29	AT375_sb16969988_1	Q	23	Yes
2010 September 2	AT375_sb1709698	Q	25	Yes
2010 September 2	AT375_sb1709503	K	27	Yes
2010 September 7	AT375_sb1710088_1	Q	22	Yes
2010 September 8	AT375_sb1709893_1	Q	25	No
2010 September 9	AT375_sb1697174_1	K	24	No

Table 2. Observational Parameter

	TUKH083	TUKH122
Phase Center RA (J2000.0)	$5^h 36^m 47^s.0$	$5^h 39^m 42^s.5$
Phase Center DEC (J2000.0)	$-6^\circ 31' 56''$	$-7^\circ 30' 09''$
Synthesized Beam at K	$4''.2 \times 3''.3$ PA = $-13^\circ.8$	$4''.2 \times 3''.1$ PA = $-1^\circ.0$
Synthesized Beam at Q	$4''.7 \times 3''.7$ PA = $-33^\circ.6$	$4''.7 \times 3''.9$ PA = $-39^\circ.7$
Primary Beam Size at K	$1''.90$	$1''.90$
Primary Beam Size at Q	$0''.99$	$0''.99$
rms Noise Level at K at 15.625 kHz (0.20 km s $^{-1}$ ) resolution	2.3 mJy beam $^{-1}$	2.6 mJy beam $^{-1}$
rms Noise Level at Q at 31.25 kHz (0.20 km s $^{-1}$ ) resolution	17 mJy beam $^{-1}$	15 mJy beam $^{-1}$

Table 3. Core and Sub-core

Line	TUKH	Suffix	RA			DEC			Flux Density	$a_{deconv}$	$b_{deconv}$	$PA_{deconv}$
			h	m	s	°	'	"	mJy beam <sup>-1</sup> km s <sup>-1</sup>	"	"	°
NH <sub>3</sub>	083	-n1	5	36	45.34	−6	31	42.0	3.5	9.6	4.8	122.5
NH <sub>3</sub>	083	-n2	5	36	45.37	−6	31	49.4	4.5	7.3	5.4	62.2
NH <sub>3</sub>	083	-n3	5	36	45.77	−6	31	55.1	4.9	3.8	1.3	30.4
NH <sub>3</sub>	083	-n4	5	36	46.43	−6	32	0.7	3.5	6.3	2.9	2.9
NH <sub>3</sub>	083	-n5	5	36	48.26	−6	32	0.3	4.2	18.2	13.3	73.7
NH <sub>3</sub>	122	-n	5	39	43.85	−7	30	26.0	10.6	56.3	14.9	147.6
NH <sub>3</sub>	122	-n1	5	39	44.57	−7	30	34.0	13.0	6.3	3.4	163.1
NH <sub>3</sub>	122	-n2	5	39	44.89	−7	30	46.8	11.8	8.5	6.5	50.4
CCS	122	-c1	5	39	41.76	−7	29	54.1	18.2	10.8	6.1	118.9
CCS	122	-c2	5	39	41.90	−7	30	12.0	18.1	6.3	4.2	60.6
CCS	122	-c3	5	39	42.77	−7	30	21.5	17.3	10.0	5.8	126.2

Table 4. Comparison between Orion cores and L1544

	TUKH122-n	TUKH122 <sup>a</sup>	TUKH123 <sup>a</sup>	L1544 <sup>b</sup>	L1544 <sup>b</sup>
$T_k$ (K)	< 15 <sup>c</sup>	< 15 <sup>c</sup>	< 15 <sup>c</sup>	9.8 <sup>d</sup>	9.8 <sup>d</sup>
adopted $T_k$ (K)	10	10	10	9.8	9.8
Molecule	NH <sub>3</sub>	CS $J = 1-0$	CS $J = 1-0$	N <sub>2</sub> H <sup>+</sup> $J = 1-0$	C <sup>18</sup> O $J = 1-0$
$\Delta v(\text{obs})$ (km s <sup>-1</sup> )	0.20	0.83	1.16	0.37	0.30
$\Delta v(\text{tot})$ (km s <sup>-1</sup> )	0.50	0.94	1.24	0.56	0.52
$R$ (pc)	0.03	0.18	0.23	0.03	0.16
$M$ ( $M_\odot$ )	1.5	33.0	74.3	2.1	9.2
$n$ (cm <sup>-3</sup> )	2.7E+05	2.4E+04	2.6E+04	2.8E+05	9.3E+03
$t_{ff}$ (yr)	6.6E+04	2.2E+05	2.1E+05	6.4E+04	3.5E+05
$l_J$ (pc)	0.03	0.08	0.08	0.02	0.13
$M_J$ ( $M_\odot$ )	0.3	0.8	0.8	0.2	1.3

<sup>a</sup>Tatematsu et al. 1993

<sup>b</sup>Tafalla et al. 1998

<sup>c</sup>Wilson et al. 1999

<sup>d</sup>Benson & Myers 1989